Static Debonding Initiation Stress of Fiber Glass Composite*

Fergyanto Efendy GUNAWAN**, Hiroomi HOMMA***,
Fenny Tri KURNIAWATI**** and Motoharu YAMAUCHI†

Mesoscale debonding initiation stress of a bundle of glass fibers and epoxy matrix under static loading is investigated. A special cylindrical bar specimen was designed for the experiment. The specimen contains a bundle of glass fibers in the center and the bundle diameters were 1 and 2 mm. The fiber diameter is 7 μm. A static tension test was performed under the displacement control. The applied load-displacement curve was recorded for each specimen and then the debonding initiation load was defined as the deviation point from the linear curve. In addition, the debonding length was measured directly from the tested specimen. Using the debonding load measured from experiment, an axisymmetric finite element analysis is performed and debonding parameters K_1 and K_2 were computed. The results show the debonding initiation is fully dominated by an opening mode rather than a sliding mode and the stress intensity factor K_1 for the debonding initiation is 2.0E+05 Pa$\sqrt{\text{m}}$. The mixed mode fracture takes place in the debonding propagation with constant mode mixity around 41.0 degree and the averaged stress intensity factors are 1.67E+05 Pa$\sqrt{\text{m}}$ and 1.41E+05 Pa$\sqrt{\text{m}}$ for the opening and the sliding mode, respectively.

Key Words: Debonding, Bimaterial, Fracture Toughness

1. Introduction

Fiber reinforced composite materials have been used in wide engineering applications. It is well known that the damages of a composite structure possibly occur in various mechanisms such as fiber fracture, matrix cracking, debonding, delamination and fiber buckling. The interface strength between the fiber and the matrix plays a very important role to transmit the load from matrix to fiber and to carry a large load as a result. Therefore, the interface is very important to keep integrity of composite structures. The interface is also one weak point of failure in a composite structure.

There are many publications concerning microscopic approach to the interface strength of a matrix and a fiber, for example Schuller[1] and Liu[2], as well as publications dealing with the interface strength in the mesoscopic level.

It is clear that the knowledge of a mesoscopic debonding behavior in a composite materials is very important to provide a bridge between microscopic interface debonding processes to the macroscopic treatment of the debonding for engineering application. However, interfacial mechanics dealing with the debonding processes is not fully developed yet to explain complicated debonding processes, because of stress complexity caused by an interface between two materials.

The fracture parameters of the interfacial crack tip in a bimaterial, such as energy release rate or J integral, stress intensity factor K, and crack opening displacement COD, have been studied extensively by many researchers. However, the fracture parameters widely changed from the one experiment to the other. Usually, the interfacial crack deforms under a mixed mode of the opening and the sliding and a mixed mode ratio changes depending on the loading configuration and the specimen geometry. Con-

* Received 29th November, 2002 (No. 02-4227)
** Department of Mechanical Engineering, Toyohashi University of Technology, 1–1 Hibarigaoka, Tempaku, Toyohashi, Aichi 441–8580, Japan.
E-mail: gunawan@mech.tut.ac.jp
*** International Cooperation Center for Engineering Education Development, Toyohashi University of Technology, 1–1 Hibarigaoka, Tempaku, Toyohashi, Aichi 441–8580, Japan
**** Light-weight Structure and Aerodynamic Laboratory, Bandung Institute of Technology, Ganesa 10, Bandung 40132, Indonesia
† Dainippon Screen MFG. Co., Ltd., 1–1 Tenjinkita-cho, Terano-agaru 4-chome, Horikawa-dori, Kamigyo-ku, Kyoto 602–0087, Japan

sidering this background, this research devises a specimen to deal with a debonding process in a simple mechanical aspect and collects basic data to clarify criteria for the debonding initiation and propagation in the framework of fracture mechanics. It is necessary to identify the fracture parameter under a single mode from the mixed mode data. Sridharan[3] developed a method based on displacement to compute a strain energy release rate for each mode. Červenka et al.[4] used extrapolation of displacement fields behind the crack tip to estimate the stress intensity factors K_1 and K_2. Ikeda[5] applied a similar technique to J-integral to compile the complex stress intensity factor from experimental data. The simplest method to compute a single-mode stress intensity factor of an interface crack was proposed by Bjerkén and Christer[6] by using a modified crack closure integral method. Because of its simplicity, this method is adopted in this work.

2. Static Debonding Experiment

2.1 Specimen

The debonding test is carried out using a cylinder bar specimen that contains a bundle of glass fibers along the axis. The specimens are fabricated in the laboratory. Glass fibers of 7 μm in diameter are bundled up into 1 mm and 2 mm diameters. The fiber bundle is placed in the center of the mold and then, the unsaturated polyester resin is poured into the mold with prudential attention to be free of air bubbles in the specimen. After the matrix is hardened, the specimen is cured at 75°C for two hours and cooled down in an oven. Mechanical properties of E-glass and unsaturated polyester are shown in Table 1. The specimen geometry and dimensions are shown in Fig. 1 and Table 2. A v-notch is machined in the middle of the length.

The macroscopic mechanical properties of the specimens are obtained based on the volume fraction of each component as shown in Table 3.

Table 1 Mechanical properties of GFRP component

	Epoxy Glass	Matrix
Young's modulus (GPa)	76.0	5.4
Poisson's ratio	0.23	0.32
Density (kg/m^3)	2510.0	1165.0

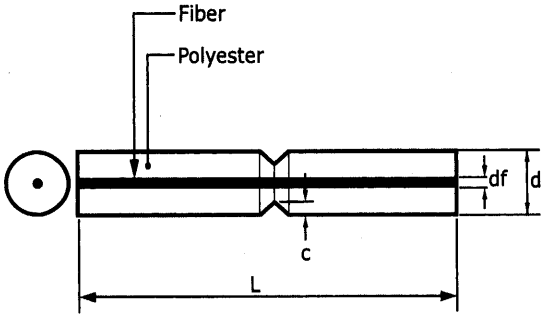

Fig. 1 Specimen geometry and dimension

2.2 Tension test

The specimen ends are firmly fixed into grips designed to prevent the slip in the grips. The grip is depicted in Fig. 2.

Load-displacement diagrams are obtained from the test. A typical load-displacement diagram is shown in Fig. 3. In figure, the stress is the nominal stress applied

Table 2 Specimen dimension

Geometry	1 mm Fiber Bundle	2 mm Fiber Bundle
Bundle dia. d_f (mm)	2.0	1.0
Specimen dia. d (mm)	9.5	9.5
Specimen length L (mm)	72.0	72.0
Depth of notch c (mm)	3.0	3.0
Notch angle (degree)	60.0	60.0

Table 3 Mechanical properties of specimen without a notch

	1 mm Fiber Bundle	2 mm Fiber Bundle
Young's mod. (GPa)	6.18	8.53
Poisson's ratio	0.32	0.32
Density (kg/m^3)	1180.0	1225.0
Fiber vol. frac. (%)	1.11	4.43

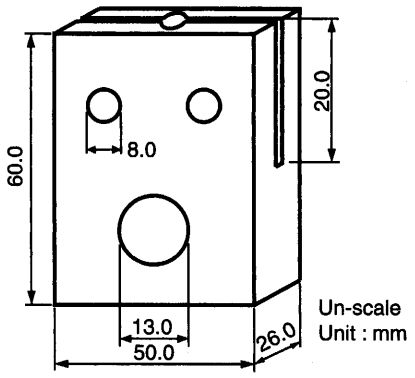

Fig. 2 Specimen holder

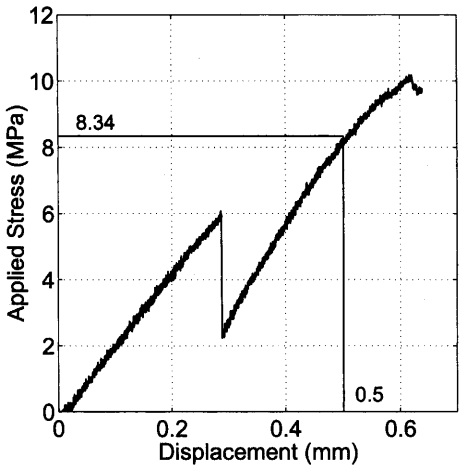

Fig. 3 Typical load-displacement diagram applied nominal stress versus deflection.

to the specimen cross section, which is the quotient of the applied load and the specimen cross section area.

3. Experimental Results

3.1 Debonding initiation

As shown in Fig. 3, the curve linearly increase with the displacement in the initial stage although at the beginning, non-linearity appears due to slight clearance between the testing fixtures and the grips. When the stress reaches the critical level, fracture initiates at the notch root, and then propagates to stop at the boundary of the matrix and the fiber bundle. When the matrix fracture takes place, the stress suddenly drops. After that, the stress increases linearly again with the displacement. At around 8.34 MPa as shown in Fig. 3, the stress-displacement curve deviates from the linear line. Beyond this point, the test was interrupted and the specimen was examined to detect the debonding. The observation indicated that the debonding between the fiber bundle and the matrix took place at this point. The debonding initiation stress was defined as 8.34 MPa for this specimen.

The debonding initiation stress is plotted for the tested specimens in Fig. 4. Eight specimens are used to obtain the critical debonding initiation stress for the 2 mm fiber bundle specimen, and twenty-seven specimens for the 1 mm fiber bundle specimen. For the 1 mm specimen, two different depths of notches are machined. As seen in figure, the debonding initiation stress is not significantly dependent on the notch depth. Therefore, the debonding initiation stress is defined as 9.0 MPa and 19.6 MPa for the 1 and 2 mm fiber bundle specimens, respectively.

3.2 Debonding propagation

After the debonding initiation, the applied stress is increased further so then the debonding area is extended. After being loaded up to a certain applied stress level, the specimen is unloaded. The specimen is observed with a digital optical microscope. The microscopic photograph is shown in Fig. 5.

As shown in Fig. 5, the debonding area is clearly identified as the white region. The debonding length is measured on the photograph then plotted as a function of the applied stress in Fig. 6.

The debonding length increases with the applied stress. In the 1 mm fiber bundle specimen, the debonding extends linearly with the applied stress, whereas in the 2 mm fiber bundle specimen, a large increment of the applied stress is necessary to expand the debonding area.

4. Numerical Analysis

4.1 Modified interface spring model and crack closure integral method

The exposition and evaluation of extension of the crack closure integral method for computing the stress intensity factor of an interface crack in a bimaterial has been developed by Bjerkén and Christer[6]. The authors also applied the method to a half body of a center cracked bimaterial specimen and an acceptable solution is achieved.

In this section, the important formulas for comput-

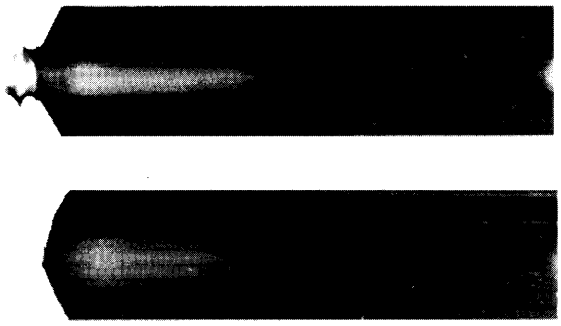

Fig. 5 Observation of debonding area

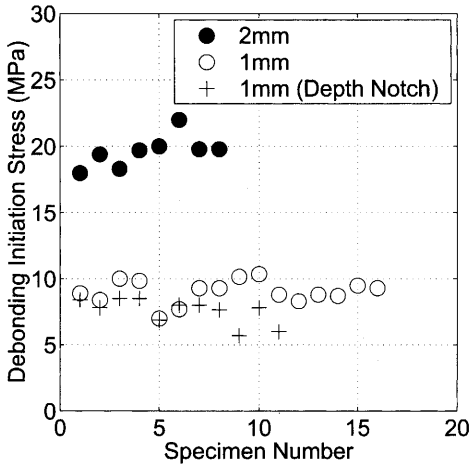

Fig. 4 Debonding initiation stress

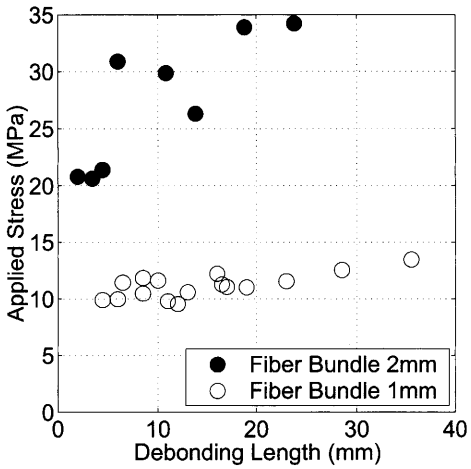

Fig. 6 Debonding length versus applied stress

ing the complex stress intensity factor are summarized and two modifications of the previous method are made.

The interface is assumed to be perfectly bonded with zero thickness. To satisfy this assumption, the coincident nodes along interface ligament are connected by equation constraint except the crack tip nodes. In this work, instead of equation constraints, those coincident nodes along ligament of interface are joined. The pair nodes at the crack tip are connected using zero length shear and normal springs. This approach will reduce the complexity in the development of the finite element mesh while the zero thickness and perfect bonding assumption are easily satisfied. In the development of a finite element mesh, the employment of equation constraint is far more complicated than joining the nodes along interfaces.

In the finite element analysis, spring forces and displacements of nodes n_1 and n_2 as depicted in Fig. 7 can be written in a complex number. The springs force can be written in complex form as follows

$$\boldsymbol{F} = F_n + jF_s \tag{1}$$

$$= |\boldsymbol{F}| e^{j\phi} \tag{2}$$

and the complex relative displacement between nodes n_1 and n_2

$$\boldsymbol{\Lambda} = \Lambda_n + j\Lambda_s \tag{3}$$

$$= |\boldsymbol{\Lambda}| e^{j\lambda} \tag{4}$$

where Λ_n and Λ_s are the relative displacement components in the normal n and the shear direction s, respectively.

The absolute value of the complex stress intensity factor is computed by[5]

$$|\boldsymbol{K}| = \sqrt{\frac{|\boldsymbol{F}||\boldsymbol{\Lambda}|}{2l_0} E^* \cosh^2(\pi\epsilon)} \tag{5}$$

with

$$\frac{1}{E^*} = \frac{1}{2}\left(\frac{1}{\bar{E}_1} + \frac{1}{\bar{E}_2}\right) \tag{6}$$

where $\bar{E}_j = E_j/(1-\nu_j^2)$ in the plane strain and $\bar{E}_j = E_j$ in the plane stress and the bi-material constant ϵ,

$$\epsilon = \frac{1}{2\pi} \ln\left[\left(\frac{\kappa_1}{\mu_1} + \frac{1}{\mu_2}\right)\Big/\left(\frac{\kappa_2}{\mu_2} + \frac{1}{\mu_1}\right)\right] \tag{7}$$

and κ_j for $j = 1, 2$,

$$\kappa_j = \begin{cases} 3-4\nu_j & \text{Plane Stress} \\ (3-4\nu_j)/(1+\nu_j) & \text{Plane Strain} \end{cases} \tag{8}$$

with μ, ν are shear modulus and Poisson's ratio, respectively.

The stress intensity factor for the normal mode and the sliding mode are computed respectively using formulas,

$$K_1 = |\boldsymbol{K}| \cos\psi \tag{9}$$

$$K_2 = |\boldsymbol{K}| \sin\psi \tag{10}$$

and an absolute stress intensity factor is computed by

$$K_{Abs.} = \sqrt{K_1^2 + K_2^2}. \tag{11}$$

The mode mixity ψ is given as

$$\psi = \frac{\phi+\lambda}{2} + \frac{\tan^{-1}(2\epsilon)}{2} - \epsilon \ln(l_0) - \frac{\omega}{2} \tag{12}$$

where ϕ and λ are computed from Eqs. (2) and (4), respectively. The bimaterial constant ϵ is computed by Eq. (7). Bjerkén et al.[6] applied a numerical integration to estimate ω as a function of ϵ for a few values of ω. In this work, their result is expressed by the following quadratic polynomial,

$$\omega = -0.3317\epsilon^2 - 2.7783\epsilon \tag{13}$$

The definition of the stress intensity factor for an interface crack was proposed by Erdogan[10] as

$$\sigma_n + j\sigma_s = \frac{K_1 + jK_2}{\sqrt{2\pi r}} \left(\frac{r}{l_0}\right)^{j\epsilon}. \tag{14}$$

Above equation shows the dependence of stress intensity factor on the characteristic length l_0. Ikeda[5] derived an equation in which the mode mixity ψ is depending on the characteristic length. He also rewrite above equation using other characteristic length.

Many ideas have been proposed for the characteristic length, such as a size closed to the process zone by Ikeda[5], the element size ahead of the crack tip by Bjerkén and Christer[6], the crack length by Sun[7] and crossing point of $\log(\sigma_n)$ and $\log(\sigma_s)$ versus $\log(r)$ on the ligament region by Tang and Zehnder[8]. In this work, the element length 1.0 mm is taken as the characteristic length.

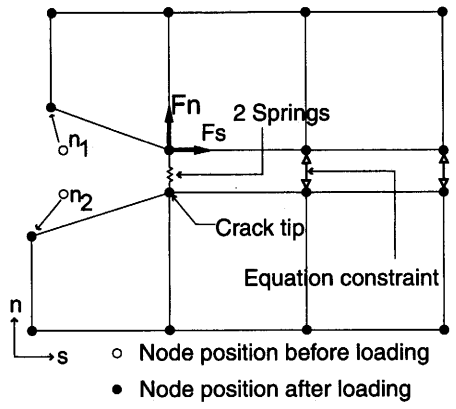

Fig. 7 Interface spring model

4.2 Fracture parameter for debonding

Accompanied with experimental results described in the previous section, a finite element analysis is performed. The ANSYS code is used for the finite element analysis. The bar is modelled using a linear axisymmetric element, since the linear element gives better estimation of a stress intensity factor than a quadratic element[9]. The boundary condition and applied loads of the finite element

model are depicted in Fig. 8. In figure, the symbol 'o' denotes the applied axisymmetric constraint.

The coincident nodes at the interface along ligament are joined except nodes at the crack tip. Both nodes are connected using shear and normal spring elements with the spring stiffness 1.0E+16 N/m for each spring. These nodes are separated in Fig. 9 for an illustration. Forty equal sized elements were placed ahead and behind the crack tip. No friction is assumed between the matrix and fiber surfaces when the bar undergoes the deformation. The analysis is performed for two types of grip forces. In the first analysis, the grip force is assumed to be zero, and in the second analysis, the grip force is assumed to be 1 N for the 1 mm and the 2 N for 2 mm fiber bundle specimen, and the force is uniformly distributed along the grip region.

The average value for the debonding initiation stress of 9.0 MPa and 19.6 MPa for the 1 mm and 2 mm fiber bundle specimen, respectively, were applied to the specimen end in the debonding initiation analysis. In the debonding propagation, the applied stress and the debonding length given in Fig. 6 were employed in the finite element analysis. The results from the finite element analysis in form of the spring forces and the relative displacement of the nodes near the crack tip are depicted in Figs. 11 and 12, respectively. These figures show the relation between the relative displacement and the spring forces for various crack length as well. Both spring forces increase significantly with the crack length up to the holder region. At around 15 mm crack length, the crack tip reached the specimen holder region, so then the spring forces decrease. The springs are playing an important role in bridging the flow of stress around the crack tip from the matrix to the fiber, and the figure shows that there

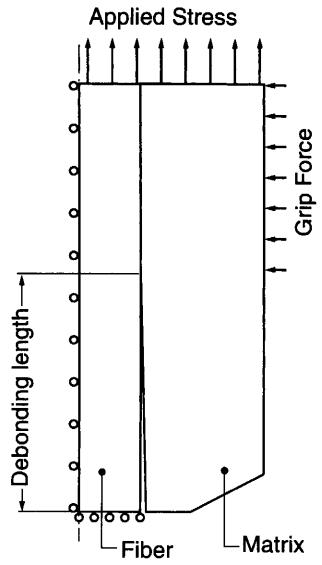

Fig. 8 Boundary condition in finite element model

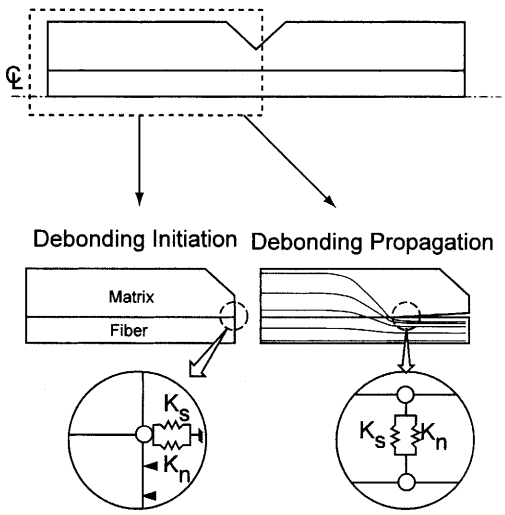

Fig. 9 Specimen model and implementation of springs to the crack tip

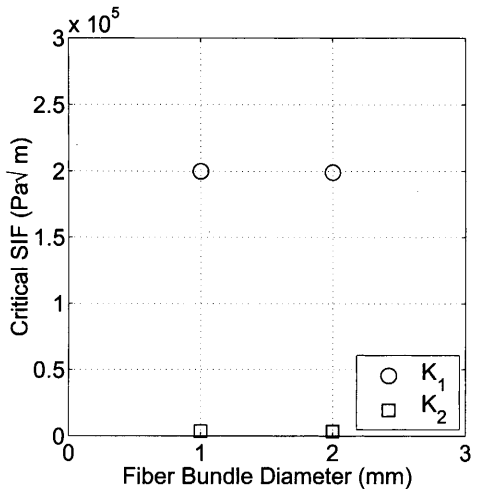

Fig. 10 Debonding initiation stress intensity factor

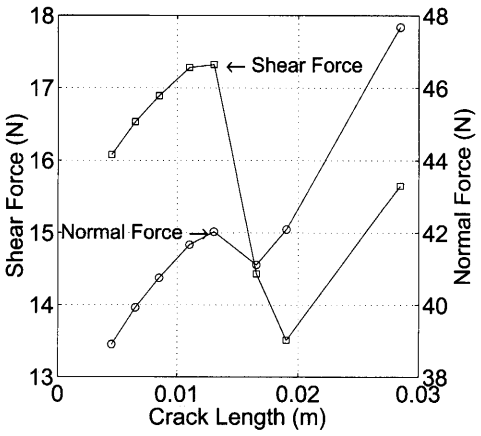

Fig. 11 Spring forces in normal and shear directions for various crack length

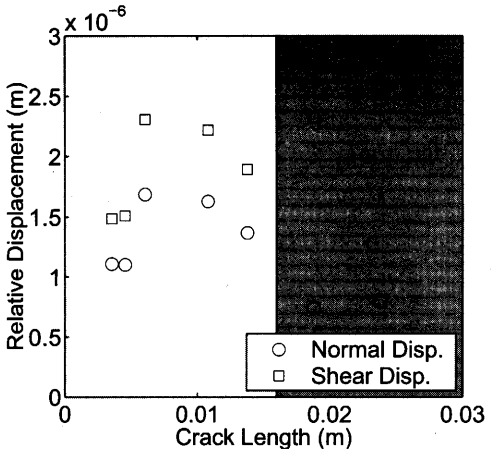

Fig. 12 Relative displacement near the crack tip

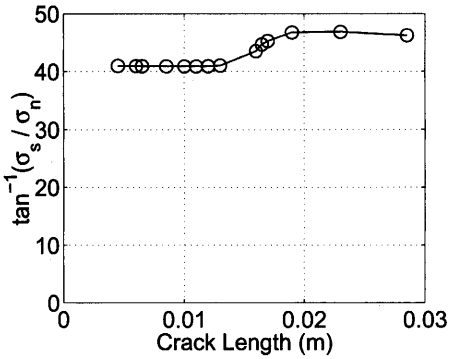

Fig. 13 Ratio of normal and shear stresses at near the crack tip

are more load passes through the springs when the crack length increase.

The finite element analysis indicates the flow of the stresses as shown in the right-bottom of Fig. 9. When the crack lies in the interface, there are no effect of the first crack on the second crack, because no stresses are remained on the first crack surface. The stresses at the matrix are transmitted to the fiber through the interface, and eventually, the stresses at the second crack tip are intensified.

For the debonding initiation, the matrix fracture at the notch tip is assumed to occur in a moment. This assumption is based on two facts. First, the ligament length of the matrix ahead of the notch tip is quite short. The ligament has nominal length about 1.25 mm for 1.0 mm fiber bundle diameter and 0.75 mm for 2.0 mm fiber bundle diameter. Second, the matrix is relatively weak and subjected to a high stress because of the stress concentration at the notch tip.

The analysis of debonding initiation is begun when the crack tip of matrix fracture rests on the interface between the fiber and the matrix. The analysis is done using the model as shown in left-bottom of Fig. 9.

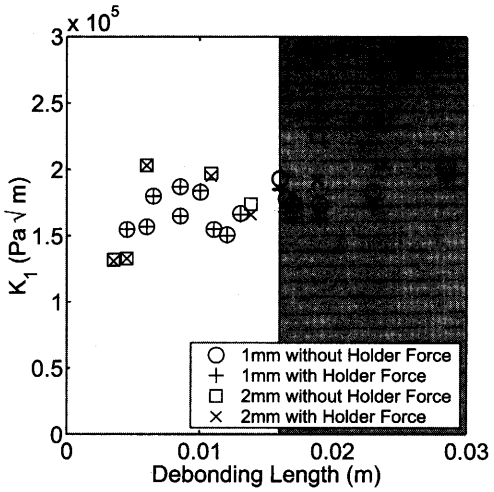

Fig. 14 Opening mode stress intensity factor versus debonding length

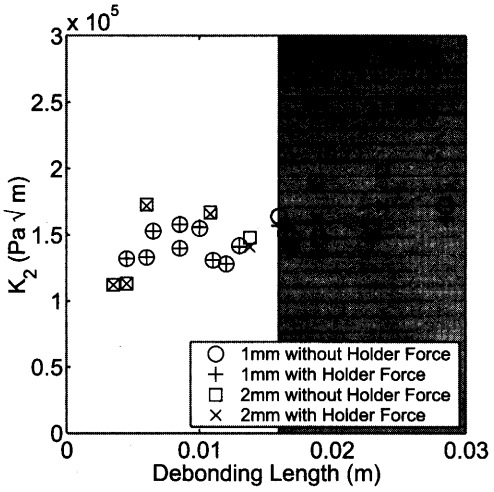

Fig. 15 Shearing mode stress intensity factor versus debonding length

By increasing the applied load, the crack tip is kinked and propagates along the matrix-fiber interface. The crack becomes the secondary crack or debonding. The model used in the finite element analysis for debonding is shown in the right-bottom of Fig. 9.

The fracture parameters K_1, K_2, $K_{Abs.}$ and mode mixity ψ shown in Figs. 14 to 17 were estimated using procedure described in section 4.1.

As shown in Fig. 10, the debonding initiation stress is fully dominated by the opening mode and the initiation debonding stress intensity factor is 2.0E+05 Pa$\sqrt{\text{m}}$. The debonding propagates in a mixed mode condition with a constant mode mixity of 41.0 degree as shown in Fig. 17. The average opening mode and shearing mode stress intensity factors are around 1.67E+05 Pa$\sqrt{\text{m}}$ and 1.41E+05 Pa$\sqrt{\text{m}}$, respectively. Observation on the relative

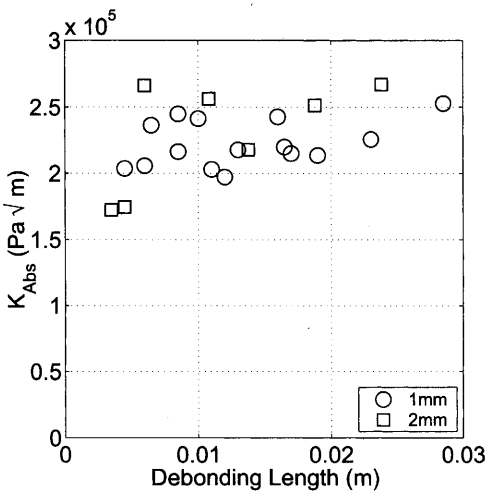

Fig. 16 Absolute stress intensity factor versus debonding length

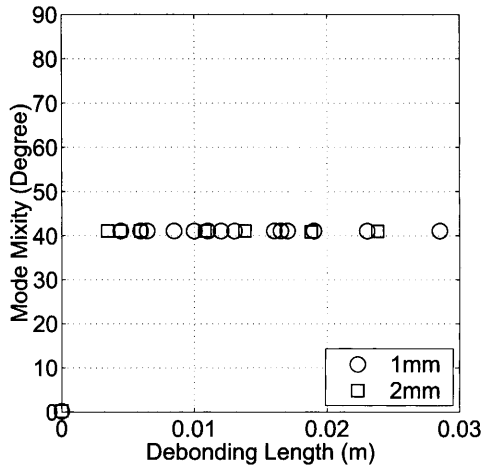

Fig. 17 Mode mixity ψ versus debonding length

displacement of first nodes behind the crack-tip in Fig. 12 also shows the mixed mode of deformation. The finite element results of the ratio of the normal to the shear stresses as given in Fig. 13 indicates the same phenomena as well.

By observing the deformation of the whole debonding surfaces, those modes of fracture should be easily understood. Debonding initiation took place around v-notch region in which the radial deformation easily took place, but when the debonding propagates to the certain length, the radial deformation was restrained by the tangential deformation. This phenomenon is schematically illustrated in Fig. 18.

As described in section 4.1, the estimation of fracture parameters are deduced from the spring forces at the crack tip and the relative displacement of the nodes behind the crack tip. Those forces and the relative displacement depend on the spring stiffness and the element size employed at the region around of the crack tip. Two

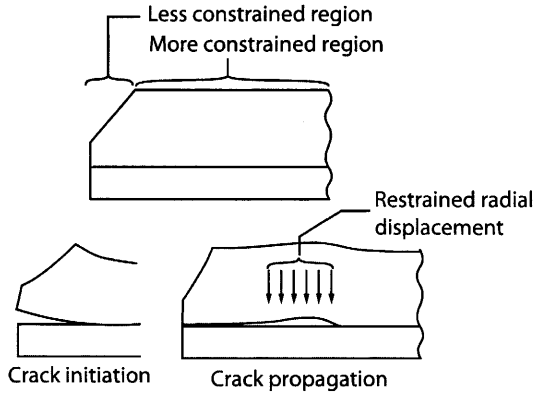

Fig. 18 Restrained radial displacement when crack propagated

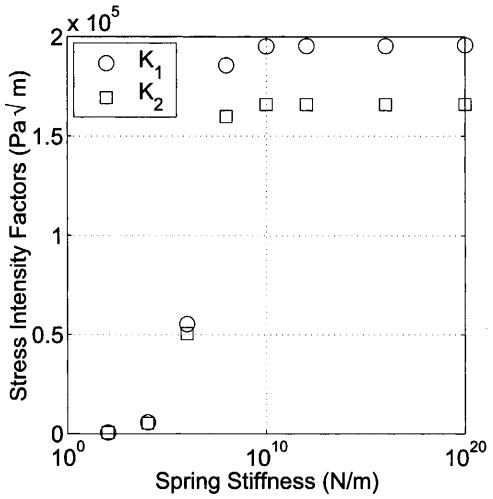

Fig. 19 Sensitivity of stress intensity factors to springs stiffness

sensitivity analyses are performed to study the effect of the both parameters on the fracture parameters. In the first sensitivity analysis, the stress intensity factor for the 2 mm fiber bundle with debonding length of 10.8 mm is computed for varying the spring stiffness from 1.0E+02 N/m to 1.0E+20 N/m. The results are shown in Fig. 19. The stress intensity factor becomes a constant for the spring stiffness greater than 1.0E+10 N/m. Thus the spring stiffness of 1.0E+16 N/m is used for all analysis. The value seems high enough to satisfy perfect bonding assumption and for the stable numerical solution.

In the second sensitivity analysis, the element size was varied in the range of 1.0, 1.3, 1.7, 2.5, 5.0, and 10.0 mm. Those element sizes were employed for the elements around the crack tip in the 2 mm fiber bundle specimen with 4.5 mm debonding length and then the fracture parameters K_1 and K_2 are computed as shown in Fig. 20. Figure 20 shows that the stress intensity factor does not sensitive to the element size.

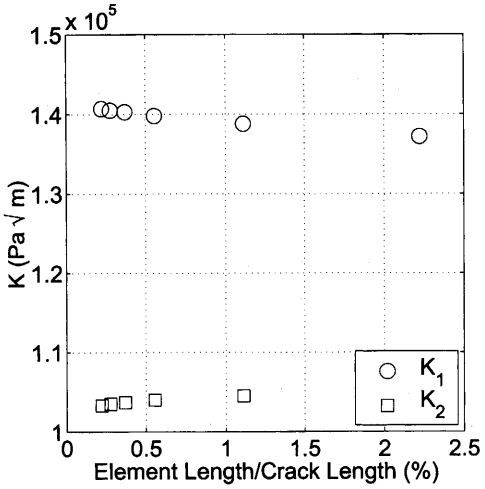

Fig. 20 Sensitivity of stress intensity factor to mesh size

5. Conclusions

The static debonding test was performed using specimen designed to detect debonding clearly and precisely. The debonding toughness parameter, a complex stress intensity factor, which was computed by use of a modified crack closure integral method for bimaterial, was applied to debonding analysis. The debonding along the fiber-matrix interface was caused under the mix mode of deformation after the debonding propagated to certain length. The debonding initiation was caused under the dominant mode I of deformation and the debonding initiation toughness was around 22.0E+05 Pa$\sqrt{m}$. In the debonding propagation under the mix mode condition, the mode I and the mode II toughness value are 1.67E+05 Pa$\sqrt{m}$ and 1.41E+05 Pa$\sqrt{m}$, respectively.

References

(1) Schuller, T., Becker, W. and Lauke, B., Analytical and Numerical Calculation of the Energy Release Rate for the Micro Bond Test, J. Adhesion, Vol.70 (1999), pp.33–56.

(2) Liu, C.H. and Nairn, J.A., Analytical and Experimental Methods for a Fracture Mechanics Interpretation of the Micro Bond Test Including the Effects Friction and Thermal Stresses, International Journal of Adhesion & Adhesives, Vol.19 (1999), pp.59–70.

(3) Sridharan, S., Displacement-Based Mode Separation of Strain Energy Release Rates for Interfacial Cracks in Bi-Material Media, International Journal of Solids and Structures, Vol.38 (2001), pp.6787–6803.

(4) Červenka, J. and Kishen, J.M.C., Mixed Mode Fracture of Cementitious Bi-Material Interfaces; Part II: Numerical Simulation, Engineering Fracture Mechanics, Vol.60, No.1 (1998), pp.95–107.

(5) Ikeda, T. and Miyazaki, N., Mixed Mode Fracture Criterion of Interface Crack between Dissimilar Materials, Engineering Fracture Mechanics, Vol.59, No.6 (1998), pp.725–735.

(6) Bjerkén, C. and Christer, P., A Numerical Method for Calculating Stress Intensity Factors for Interface Cracks in Bi-Materials, Engineering Fracture Mechanics, Vol.68 (2001), pp.235–246.

(7) Sun, C.T. and Jih, C.J., On Strain Energy Release Reates for Interfacial Cracks in Bi-Material Media, Engineering Fracture Mechanics, Vol.28 (1987), pp.13–20.

(8) Tang, S. and Zehnder, A.T., Nickel-Alumina Interfacial Fracture Toughness Using Thick Foil Technique, Engineering Fracture Mechanics, Vol.69 (2002), pp.701–715.

(9) Rybicki, E.F. and Kanninen, M.F., A Finite Element Calculation of Stress Intensity Factors by a Modified Crack Closure Integral, Int. J. Frac. Mech., Vol.9 (1977), pp.931–938.

(10) Erdogan, F., Stress Distribution in Bonded Dissimilar Materials with Cracks, Transactions of the ASME Series E, Journal of Applied Mechanics, Vol.32 (1963), pp.403–410.